Critical weight statistics of the random energy model and of the directed polymer on the Cayley tree

Cécile Monthus and Thomas Garel
Service de Physique Théorique, CEA/DSM/SPhT, CNRS, 91191 Gif-sur-Yvette cedex, France
(Received 2 March 2007; published 25 May 2007)

We consider the critical point of two mean-field disordered models: (i) the random energy model (REM), introduced by Derrida as a mean-field spin-glass model of N spins and (ii) the directed polymer of length N on a Cayley Tree (DPCT) with random bond energies. Both models are known to exhibit a freezing transition between a high-temperature phase where the entropy is extensive and a low-temperature phase of finite entropy, where the weight statistics coincides with the weight statistics of Lévy sums with index $\mu=T/T_c<1$. In this paper, we study the weight statistics at criticality via the entropy $S=-\Sigma w_i \ln w_i$ and the generalized moments $Y_k=\Sigma w_i^k$, where the w_i are the Boltzmann weights of the 2^N configurations. In the REM, we find that the critical weight statistics is governed by the finite-size exponent $\nu=2$: the entropy scales as $\bar{S}_N(T_c)\sim N^{1/2}$, the typical values $e^{\overline{\ln Y_k}}$ decay as $N^{-k/2}$, and the disorder-averaged values $\overline{Y_k}$ are governed by rare events and decay as $N^{-1/2}$ for any $k>1$. For the DPCT, we find that the entropy scales similarly as $\bar{S}_N(T_c)\sim N^{1/2}$, whereas another exponent $\nu'=1$ governs the Y_k statistics: the typical values $e^{\overline{\ln Y_k}}$ decay as N^{-k}, and the disorder-averaged values $\overline{Y_k}$ decay as N^{-1} for any $k>1$. As a consequence, the asymptotic probability distribution $\bar{\pi}_{N=\infty}(q)$ of the overlap q, in addition to the delta function $\delta(q)$, which bears the whole normalization, contains an isolated point at $q=1$, as a memory of the delta peak $(1-T/T_c)\delta(q-1)$ of the low-temperature phase $T<T_c$. The associated value $\bar{\pi}_{N=\infty}(q=1)$ is finite for the DPCT, and diverges as $\bar{\pi}_{N=\infty}(q=1)\sim N^{1/2}$ for the REM.

DOI: 10.1103/PhysRevE.75.051119 PACS number(s): 02.50.−r, 05.40.Fb, 75.10.Nr

I. INTRODUCTION

Spin glasses [1,2] and directed polymers in random media [3] are two kinds of disordered models where the relations between finite-dimensional models and mean-field models have remained controversial over the years. For the directed polymer in a random medium of dimension $1+d$, with $d=3$ where a localization-delocalization transition occurs, we have recently found numerically that the weight statistics is multifractal at criticality [4], in close analogy with models of the quantum Anderson localization transition, where the multifractality of critical wave functions is well established [5,6]. In this paper, our aim is to study the critical weight statistics in the mean-field version of the model, namely, the directed polymer on a Cayley tree (DPCT) [7–9]. This model presents many similarities [7,8] with the random energy model (REM), introduced by Derrida as a mean-field spin-glass model [10]: both models are known to exhibit a freezing transition between a high-temperature phase where the thermodynamic observables coincide with their extensive annealed values, and a low-temperature phase of finite entropy, in which the weight statistics [11,12] coincides with the weight statistics of Lévy sums with index $\mu=T/T_c<1$ [13]. Therefore we also study the weight statistics of the REM at criticality, as well as in Lévy sums at the critical value $\mu_c=1$, to compare with the results for the directed polymer on a Cayley tree. We find that the three models have different critical finite-size properties.

The paper is organized as follows. In Sec. II, we recall the main properties of the random energy model and of the directed polymer on a Cayley tree. We then study in parallel the weight statistics at criticality for the two models: we describe the properties of the entropy in Sec. III, the decay of disorder-averaged values $\overline{Y_k}$ in Sec. IV, and the decay of typical values $Y_k^{typ}=e^{\overline{\ln Y_k}}$ in Sec. V. To explain the differences between averaged and typical values, we discuss in Sec. VI the probability distributions of the maximal weight w_{max} and of Y_2 over the samples, with a special emphasis on the rare events that govern average values. Section VII is devoted to the finite-size properties of the overlap distribution at criticality. Section VIII contains our conclusions. For clarity, the weight statistics of Lévy sums is discussed separately in the Appendixes: We first recall in Appendix A the results for $\mu<1$, and we describe the critical case $\mu_c=1$ in Appendix B.

II. MODELS AND OBSERVABLES

A. Reminder of the random energy model

The random energy model, introduced in the context of spin glasses [10], is defined by the partition function

$$Z_N=\sum_{i=1}^{2^N} e^{-\beta E_i} \tag{1}$$

where the energies E_i of the 2^N configurations of N spins are assumed to be independent random variables drawn from the Gaussian distribution

$$P_N(E)=\frac{1}{\sqrt{\pi N}}e^{-E^2/N}. \tag{2}$$

This model presents a freezing transition at [10]

$$T_c=\frac{1}{2\sqrt{\ln 2}}, \tag{3}$$

and we now briefly recall the main properties of the high- and low-temperature phases.

1. High-temperature phase

In the high-temperature phase $T \geqslant T_c$, the free energy per spin coincides with the annealed free energy [10]

$$f(T > T_c) = f_{ann}(T) = -T \ln 2 - \frac{1}{4T}. \tag{4}$$

As a consequence, the entropy per spin vanishes linearly at the transition,

$$s(T > T_c) = s_{ann}(T) = \ln 2 - \frac{1}{4T^2} \underset{T \to T_c^+}{\propto} (T - T_c), \tag{5}$$

and the specific heat per spin remains finite,

$$c(T > T_c) = c_{ann}(T) = \frac{1}{2T^2} \underset{T \to T_c^+}{\simeq} c(T_c^+) = 2 \ln 2. \tag{6}$$

2. Low-temperature phase

From the thermodynamic point of view, the low-temperature phase $T < T_c$ is completely frozen, with a constant free energy per spin [10]

$$f(T \leqslant T_c) = -\sqrt{\ln 2}. \tag{7}$$

As a consequence, the entropy per spin vanishes in the whole low-temperature phase,

$$s(T \leqslant T_c) = 0, \tag{8}$$

as well as the specific heat per spin,

$$c(T < T_c) = 0. \tag{9}$$

To understand better the properties of this low-temperature phase, it is convenient to study the statistical properties of the configuration weights in the partition function [Eq. (1)]

$$w_i = \frac{e^{-\beta E_i}}{Z_N}. \tag{10}$$

It turns out that their statistics is in direct correspondence with Lévy sums of index $0 < \mu = T/T_c < 1$ [13] (see Appendix A for more details). In particular, the moments

$$Y_k = \sum_{i=1}^{2^N} w_i^k \tag{11}$$

have for disorder averages [13]

$$\overline{Y_k} = \frac{\Gamma(k - \mu(T))}{\Gamma(k)\Gamma(1 - \mu(T))} \quad \text{with } \mu(T) = \frac{T}{T_c}. \tag{12}$$

The density $f(w)$ giving rise to these moments,

$$\overline{Y_k} = \int_0^1 dw\, w^k f(w), \tag{13}$$

reads [13]

$$f(w) = \frac{w^{-1-\mu}(1-w)^{\mu-1}}{\Gamma(\mu)\Gamma(1-\mu)} \tag{14}$$

and represents the averaged number of terms of weight w. This density is nonintegrable as $w \to 0$, because in the limit $N \to \infty$ the number of terms of vanishing weight diverges. The normalization corresponds to

$$\overline{Y_{k=1}} = \int_0^1 dw\, w f(w) = 1. \tag{15}$$

In particular, as the transition is approached $\mu = T/T_c \to 1^-$ these disorder-averaged moments all vanish linearly for $k > 1$

$$\overline{Y_k} \underset{T \to T_c^-}{\propto} (T_c - T). \tag{16}$$

The link between these weight properties and the thermodynamics is via the total entropy [14]

$$S_N = -\sum_{i=1}^{2^N} w_i \ln(w_i) = -\left[\partial_k \sum_{i=1}^{2^N} w_i^k \right]_{k \to 1} = -[\partial_k Y_k]_{k \to 1}. \tag{17}$$

From Eq. (12), the disorder-averaged value over the samples reads

$$\bar{S}_N(T < T_c) = -[\partial_k \bar{Y}_k]_{k \to 1} = \Gamma'(1) - \frac{\Gamma'(1 - \mu(T))}{\Gamma(1 - \mu(T))}. \tag{18}$$

In the critical region $T \to T_c^-$, the entropy per spin presents the following finite-size scaling behavior:

$$\overline{s_N(T)} \equiv \frac{\overline{S_N(T)}}{N} \underset{T \to T_c^-}{\propto} \frac{1}{N(T_c - T)}. \tag{19}$$

Similarly, the disorder-averaged specific heat per spin follows:

$$\overline{c_N(T)} \equiv \frac{\overline{C_N(T)}}{N} \underset{T \to T_c^-}{\propto} \frac{1}{N(T_c - T)^2}. \tag{20}$$

These finite-size scaling behaviors are in agreement with the more detailed finite-size corrections of the free energy computed in [10].

B. Reminder of the directed polymer on a Cayley tree

The directed polymer on a Cayley tree with disorder was introduced in [7] as a mean-field version of the directed polymer in a random medium [3]. The model is defined by the partition function

$$Z_N = \sum_{\mathcal{C}} e^{-\beta E(\mathcal{C})}, \tag{21}$$

where the 2^N configurations $\mathcal{C}$ are the paths of N steps on a Cayley tree with coordination number $K = 2$. The energy $E(\mathcal{C})$ of a path is the sum of the energies of the visited bonds. Each bond has a random energy drawn independently, for instance with the Gaussian distribution

$$\rho(\epsilon) = \frac{1}{\sqrt{2\pi}} e^{-\epsilon^2/2}. \tag{22}$$

As in Eq. (10), it is convenient to consider the configuration weights $w(\mathcal{C}) = e^{-\beta E(\mathcal{C})}/Z_N$ in the partition function [Eq. (21)] and the associated moments Y_k [Eq. (11)].

1. Similarities with the random energy model

This model presents many similarities [7,8] with the random energy model described above. It presents a freezing transition at

$$T_c = \frac{1}{\sqrt{2 \ln 2}}. \tag{23}$$

The free energy per step coincides with the annealed free energy above T_c and is completely frozen below,

$$f(T) = \begin{cases} f_{ann}(T) = -T \ln 2 - \dfrac{1}{2T} & \text{for } T \geqslant T_c, \quad (24) \\ -\sqrt{2 \ln 2} & \text{for } T \leqslant T_c. \quad (25) \end{cases}$$

So, at the thermodynamic level, all properties are the same as in the REM: The entropy per step vanishes linearly at the transition [Eq. (5)], and the specific heat per step presents a jump [Eq. (6)]. From the finite-size behavior of the free energy for $T < T_c$ [Eq. (76) of [8]], one obtains by differentiation with respect to the temperature that the entropy per step and the specific heat per step have the same finite-size scaling as in the REM [Eqs. (19) and (20)],

$$\overline{s_N(T)} \equiv \overline{\frac{S_N(T)}{N}} \underset{T \to T_c^-}{\propto} \frac{1}{N(T_c - T)}, \tag{26}$$

$$\overline{c_N(T)} \equiv \overline{\frac{C_N(T)}{N}} \underset{T \to T_c^-}{\propto} \frac{1}{N(T_c - T)^2}. \tag{27}$$

It turns out that setting aside even these thermodynamic quantities, the two models are still very similar. In [7], it was shown that, in the limit $N \to \infty$, the distribution of the overlap q between two walks on the same disordered tree is simply the sum of two δ peaks at $q=0$ and 1 in the whole low-temperature phase [7]:

$$\pi(q) = (1 - Y_2)\delta(q) + Y_2 \delta(q - 1), \tag{28}$$

and the distribution of Y_2 over the samples is exactly the same as in the random energy model [7]. In particular, its averaged value reads [7]

$$\overline{Y_2(T)} = 1 - \frac{T}{T_c}. \tag{29}$$

2. Differences from the random energy model

As explained in detail in [8], the difference from the random energy model is that the directed polymer on a Cayley tree corresponds to a generalized random energy model (GREM) with $p=N$ levels, whereas the REM corresponds to the case of a GREM with $p=1$ level. This induces some differences for the finite-size properties of the free energy [8]. The conclusion of [8] is that the finite-size scaling behavior of the REM only involves the product $(T_c - T)N^{1/\nu}$ with

$$\nu = 2, \tag{30}$$

whereas for the Cayley tree, the situation is more subtle, and the product $(T_c - T)N^{1/\nu'}$ with another exponent

$$\nu' = 1 \tag{31}$$

also appears. As a consequence, even if the weight statistics is the same in the low-temperature phase of the two models, their critical properties might be different, as we will indeed find in the following.

C. Numerical details

The numerical results given in the following sections for the REM and the DPCT have been obtained for the following sizes N (with 2^N configurations) and the corresponding numbers $n_s(N)$ of disordered samples

$$N = 5 - 14, 16, 18, 20, \tag{32}$$

$$n_s(N) = 10^7, 4 \times 10^6, 10^6, 4 \times 10^5. \tag{33}$$

III. ENTROPY AT CRITICALITY

A. Disorder-averaged entropy at criticality

We have recalled in the previous section that both for the random energy model and for the directed polymer on the Cayley tree, the freezing transition corresponds to a jump in the intensive specific heat,

$$\overline{c_N(T > T_c)} \underset{T \to T_c^+}{\simeq} \text{const}, \tag{34}$$

$$\overline{c_N(T < T_c)} \underset{T \to T_c^-}{\simeq} \frac{1}{N(T_c - T)^2}. \tag{35}$$

The finite-size scaling thus involves the exponent $\nu=2$,

$$\overline{c_N(T)} = \mathcal{C}((T_c - T)N^{1/\nu}) \quad \text{with } \nu = 2. \tag{36}$$

For the REM, the explicit form of the scaling function can be obtained from Eq. (64) of [8].

Similarly, the total disorder-averaged entropy has the following behaviors on both sides of the transition:

$$\overline{S_N(T > T_c)} \underset{T \to T_c^+}{\simeq} N(T - T_c), \tag{37}$$

$$\overline{S_N(T < T_c)} \underset{T \to T_c^-}{\simeq} \frac{1}{T_c - T}. \tag{38}$$

One thus expects the following finite-size scaling form:

$$\overline{S_N(T)} = N^{1/2} \mathcal{S}((T_c - T)N^{1/\nu}) \quad \text{with } \nu = 2. \tag{39}$$

At criticality, we thus expect both for the REM and for the directed polymer on the Cayley tree

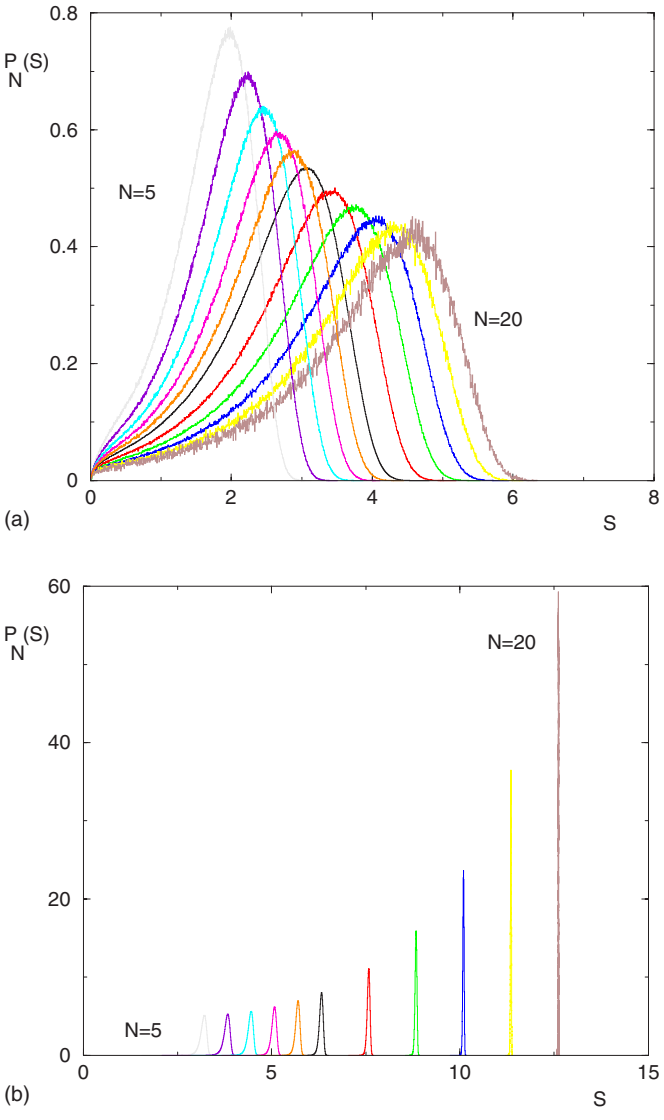

FIG. 1. (Color online) REM: entropy probability distribution $P_N(S)$ for sizes $N=5,6,7,8,9,10,12,14,16,18,20$. (a) At T_c, the distribution remains broad around the averaged value $\bar{S} \propto N^{1/2}$, with a slow decay of rare events of small entropy $S \sim 0$. (b) At $T=2 > T_c$, the width around the average value $\bar{S}=Ns_{ann}(T)$ decays exponentially in N, in agreement with Ref. [15].

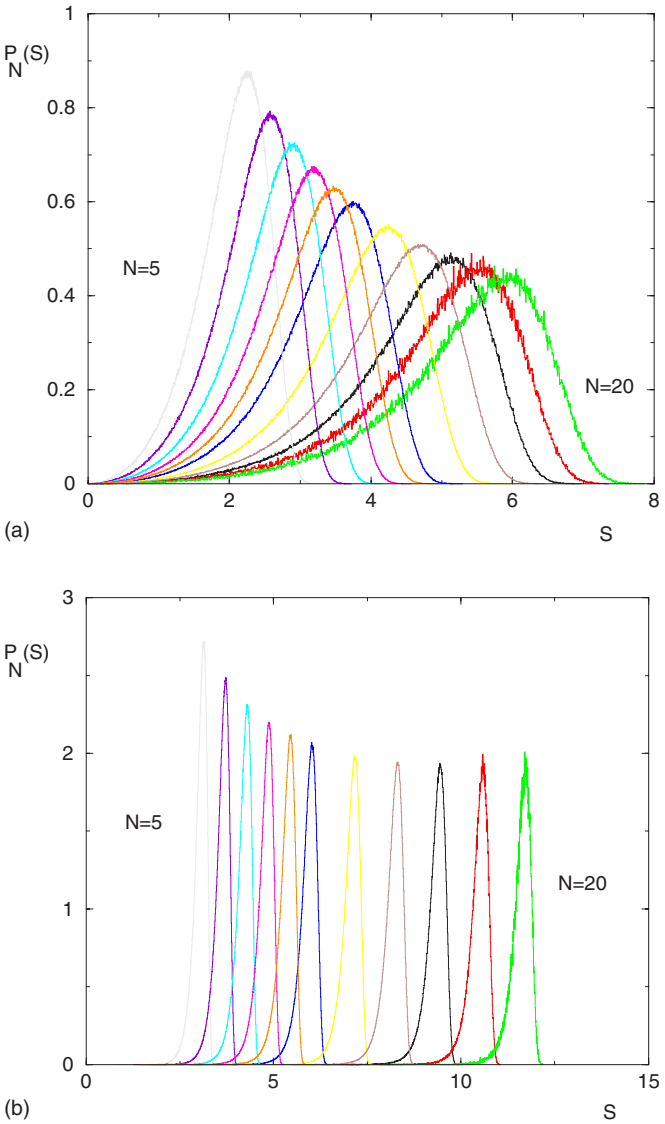

FIG. 2. (Color online) DPCT: entropy probability distribution $P_N(S)$ for sizes $N=5,6,7,8,9,10,12,14,16,18,20$. (a) At T_c, the distribution remains broad around the averaged value $\bar{S} \propto N^{1/2}$. The statistics of rare events in the region $S \sim 0$ is different from that in the REM [see Fig. 1(a)]. (b) At $T=2 > T_c$. the width around the average value $\bar{S}=Ns_{ann}(T)$ converges toward a constant, in contrast with the REM [see Fig. 1(b)].

$$\overline{S_N(T_c)} \propto N^{1/2}, \tag{40}$$

in agreement with our numerical simulations for both models.

B. Entropy distribution at criticality

We show in Figs. 1 and 2 the probability distribution $P_N(S)$ of the entropy S for the REM and for the DPCT, respectively, both at criticality and in the high-temperature phase for comparison. At criticality, $P_N(S)$ remains broad around the averaged value $\bar{S} \propto N^{1/2}$, with a slow decay of rare events of small entropy $S \sim 0$. The comparison of Figs. 1(a) and 2(a) shows that these rare finite samples that are still "frozen" at T_c do not obey the same statistics in the REM and in the DPCT (see the more detailed discussion on rare events in Sec. VI C). In the high-temperature phase, the width around the average value $\bar{S}=Ns_{ann}(T)$ decays exponentially in N in the REM [15], as shown in Fig. 1(b), whereas it converges toward a constant in the DPCT, as shown in Fig. 2(b).

IV. DECAY OF DISORDER-AVERAGED VALUES $\overline{Y_K}(N)$ AT CRITICALITY

A. Special case $k=2$

As already mentioned in Eq. (29), for $k=2$, the explicit expression of $\overline{Y_2}(N)$ is particularly simple in the low-temperature phase,

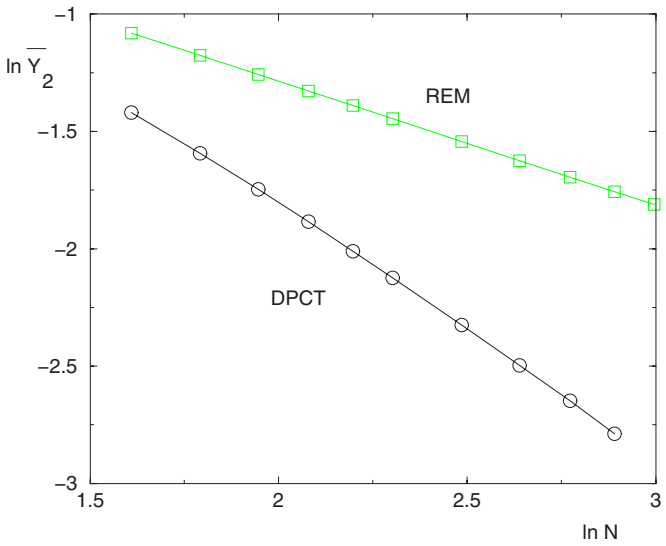

FIG. 3. (Color online) At criticality, the slope of $\ln \overline{Y_2}(N,T_c)$ as a function of $(\ln N)$ (here $5 \leqslant N \leqslant 20$) is of order $1/\nu=0.5$ for the REM (□) and of order $1/\nu'=1$ for the DPCT (○).

$$\overline{Y_2(T<T_c)} = \frac{T_c - T}{T_c}. \tag{41}$$

In the REM where the only finite-size scaling exponent is $\nu=2$ [Eq. (30)], one thus expects at criticality

$$[\overline{Y_2(T_c,N)}]_{REM} \underset{N\to\infty}{\propto} \frac{1}{N^{1/2}}, \tag{42}$$

in agreement with our numerical simulations, as shown in Fig. 3. For the DPCT, however, we find numerically that the decay of $\overline{Y_2}$ is governed by the exponent $\nu'=1$ [Eq. (31)] at criticality

$$[\overline{Y_2(T_c,N)}]_{DPCT} \underset{N\to\infty}{\propto} \frac{1}{N} \tag{43}$$

as shown in Fig. 3.

B. Other values of k

For arbitrary k, the explicit value [Eq. (12)] can be expanded in $(T_c-T)/T_c$ as follows:

$$\overline{Y_k}(T<T_c) = \frac{(T_c - T)}{(k-1)T_c}[1 + O(T_c - T)]. \tag{44}$$

For the REM where the only finite-size scaling exponent is $\nu=2$ [Eq. (30)], one thus expects at criticality

$$[\overline{Y_k(T_c,N)}]_{REM} = \frac{1}{(k-1)N^{1/2}}\left[1 + O\left(\frac{1}{N^{1/2}}\right)\right], \tag{45}$$

in agreement with our numerical simulations. For the DPCT, we find numerically that it is the exponent $\nu'=1$ [Eq. (31)] that governs the critical behavior

$$[\overline{Y_k(T_c,N)}]_{DPCT} \propto \frac{1}{N}\left[1 + O\left(\frac{1}{N}\right)\right]. \tag{46}$$

V. DECAY OF TYPICAL VALUES $Y_K^{TYP}(N) = e^{\overline{\ln Y_k}}$ AT CRITICALITY

From the explicit expression Eq. (A19) of $\overline{\ln Y_k}$ in the low-temperature phase with $\mu=T/T_c$, one obtains the following expansion in (T_c-T):

$$\overline{\ln Y_k} = k[1 + a_1(T_c - T) + O((T_c - T)^2)]\ln(T_c - T) + b_0 + b_1(T_c - T) + O((T_c - T)^2). \tag{47}$$

For the REM where the only finite-size scaling exponent is $\nu=2$ [Eq. (30)], one thus expects at criticality

$$[\overline{\ln Y_k(T_c,N)}]_{REM} \propto -\frac{k}{2}\left[1 + O\left(\frac{1}{\sqrt{N}}\right)\right]\ln N + \text{const} + O\left(\frac{1}{\sqrt{N}}\right), \tag{48}$$

in agreement with our numerical simulations.

For the DPCT, we find that it is the exponent $\nu'=1$ that governs the decay of typical weights

$$[\overline{\ln Y_k(T_c,N)}]_{DPCT} \propto -k\left[1 + O\left(\frac{1}{N}\right)\right]\ln N + \text{const} + O\left(\frac{1}{N}\right). \tag{49}$$

To summarize, the exponents governing the decay of typical values are exactly linear in k in both models,

$$[Y_k^{typ}(N)]_{REM} = e^{\overline{\ln Y_k}} \propto \frac{1}{N^{k/2}} \tag{50}$$

and

$$[Y_k^{typ}(N)]_{DPCT} = e^{\overline{\ln Y_k}} \propto \frac{1}{N^k}, \tag{51}$$

in contrast with disorder-averaged values, where the exponents do not depend on k [Eqs. (45) and (46)]. To explain this difference, we now discuss the histograms of w_{max} and of Y_2 at criticality.

VI. PROBABILITY DISTRIBUTIONS OF w_{max} AND OF Y_2 AT CRITICALITY

A. Probability distribution of $w_{max}(N)$ at criticality

For each sample, we consider the maximal weight

$$w_{max} = \max_i(w_i) \tag{52}$$

among the 2^N configurations. We show in Figs. 4 and 5 the probability distribution $P_N(\ln w_{max})$ over the samples for the REM and the DPCT, both at criticality and in the high-temperature phase for comparison. At criticality, $P_N(\ln w_{max})$ remains broad around the averaged value,

$$\overline{\ln w_{max}} \simeq \begin{cases} -\frac{1}{2}(\ln N) + \cdots & \text{for the REM}, \quad (53) \\ -(\ln N) + \cdots & \text{for the DPCT}, \quad (54) \end{cases}$$

with a slow decay of rare events near the origin, $\ln w_{max} \sim 0$. Again, as for the entropy distribution [see Figs. 1(a) and

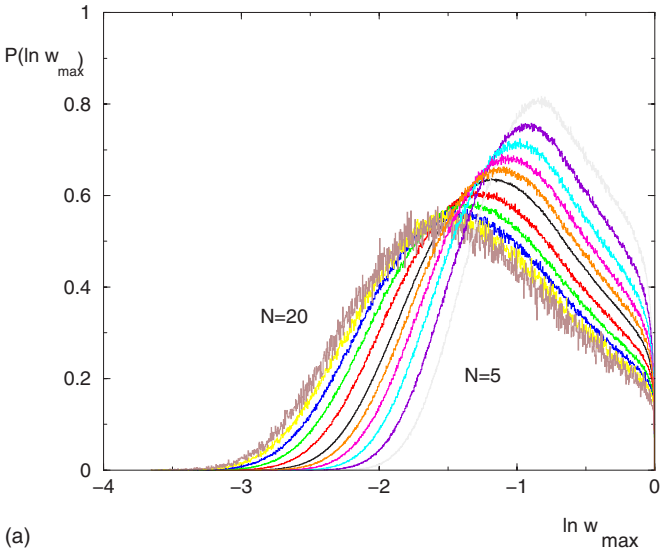

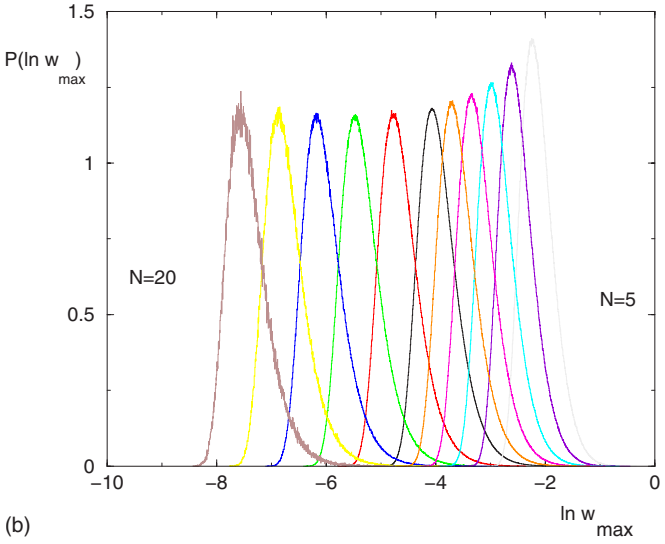

FIG. 4. (Color online) REM: Probability distribution $P_N(\ln w_{max})$ of the maximal weight among the 2^N configurations, for sizes $N=5,6,7,8,9,10,12,14,16,18,20$. (a) At T_c, the distribution remains broad around the averaged value $\ln w_{max} \simeq -(\ln N)/2$, with a slow decay of rare events near the origin, $\ln w_{max} \sim 0$. (b) At $T=2>T_c$, the width around the average value $\ln w_{max} \propto -N$ converges toward a constant.

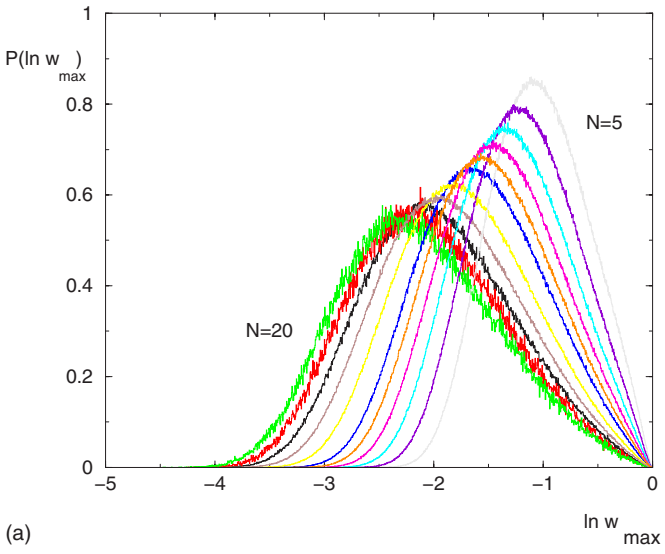

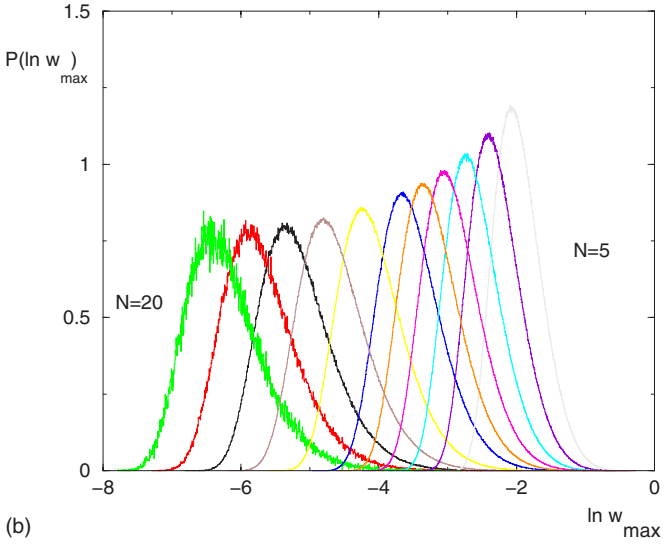

FIG. 5. (Color online) DPCT: Probability distribution $P_N(\ln w_{max})$ of the maximal weight among the 2^N configurations, for sizes $N=5,6,7,8,9,10,12,14,16,18,20$. (a) At T_c, the distribution remains broad around the averaged value $\ln w_{max} \simeq -(\ln N)$, with a slow decay of rare events near the origin, $\ln w_{max} \sim 0$. (b) At $T=2>T_c$, the width around the average value $\ln w_{max} \propto -N$ converges toward a constant.

2(a)], the statistics of these rare still frozen samples is not the same in the REM and in the DPCT as shown in Figs. 4(a) and 5(a). In the high-temperature phase, the width around the average value $\ln w_{max} \propto -N$ converges toward a constant in both models, as shown in Figs. 4(b) and 5(b).

B. Probability distribution of Y_2 at criticality

We show in Figs. 6 and 7 the probability distribution $P_N(\ln Y_2)$ over the samples for the REM and the DPCT, both at criticality and in the high-temperature phase for comparison. At criticality, $P_N(\ln Y_2)$ remains broad around the averaged value,

$$\overline{\ln Y_2} \simeq \begin{cases} -(\ln N) + \cdots & \text{for the REM,} \quad (55) \\ -2(\ln N) + \cdots & \text{for the DPCT,} \quad (56) \end{cases}$$

with again a different decay of rare events near the origin, $\ln Y_2 \sim 0$. In the high-temperature phase, the width around the average value $\ln Y_2 \propto -N$ converges toward zero for the REM, as shown in Fig. 6(b), and toward a finite constant for the DPCT, as shown in Fig. 7(b).

As a final remark, it is interesting to compare the probability distribution of $\ln Y_2$ at criticality for the directed polymer on the Cayley tree [Fig. 7(a)] and in dimension $1+3$ (see Fig. 3a of [4]), where as N grows, the distribution simply shifts along the x axis with a fixed shape.

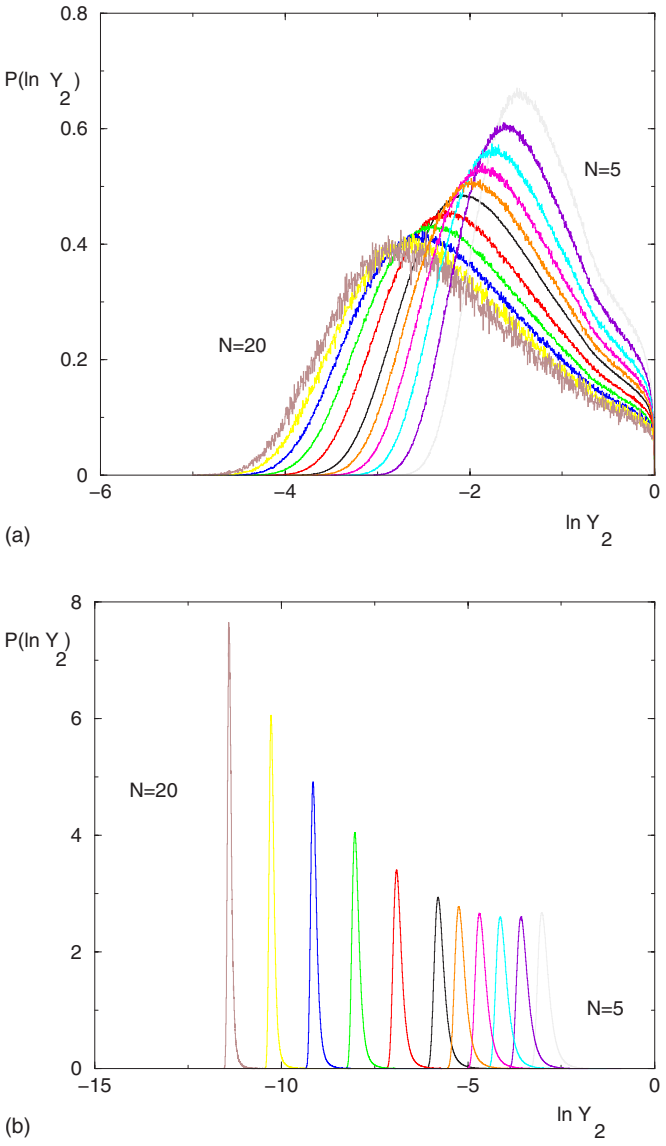

FIG. 6. (Color online) REM: Probability distribution $P_N(\ln Y_2)$ for sizes $N=5,6,7,8,9,10,12,14,16,18,20$. (a) At T_c, the distribution remains broad around the averaged value $\overline{\ln Y_2} \simeq -(\ln N)$, with a slow decay of rare events near the origin, $\ln Y_2 \sim 0$. (b) At $T=2>T_c$, the width around the average value $\overline{\ln Y_2} \propto -N$ converges toward zero.

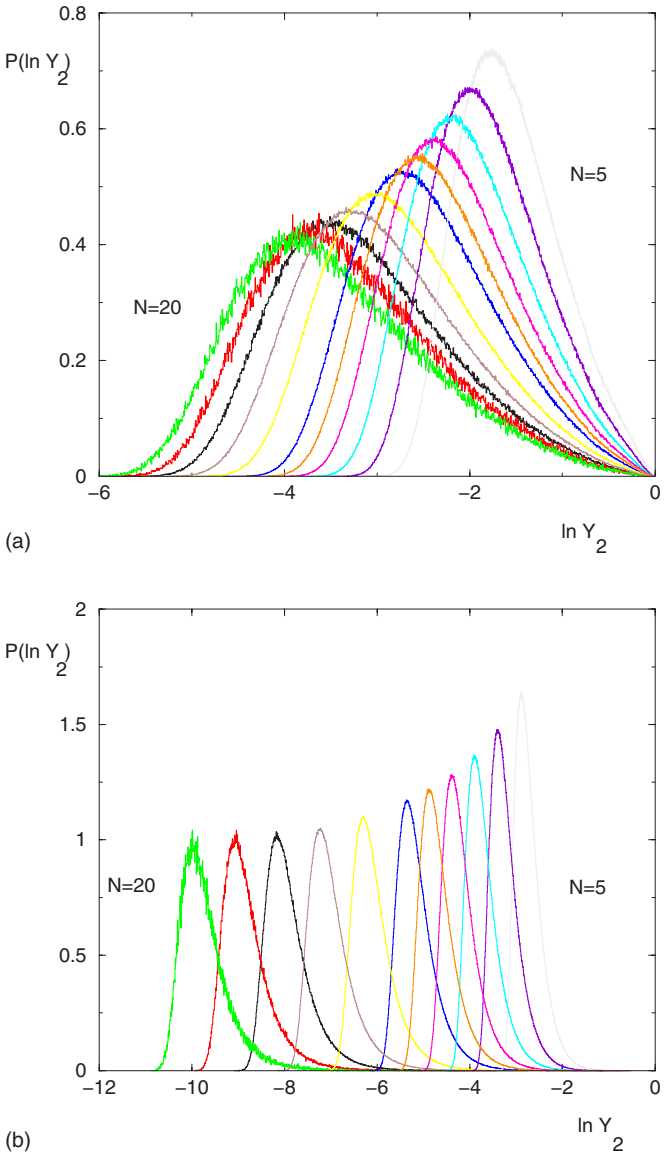

FIG. 7. (Color online) DPCT: Probability distribution $P_N(\ln Y_2)$ for sizes $N=5,6,7,8,9,10,12,14,16,18,20$. (a) At T_c, the distribution remains broad around the averaged value $\overline{\ln Y_2} \simeq -2(\ln N)$, with a slow decay of rare events near the origin, $\ln Y_2 \sim 0$. (b) At $T=2>T_c$, the width around the average value $\overline{\ln Y_2} \propto N$ converges toward a constant.

C. Rare events where $w_{max} \sim 1$ and $Y_2 \sim 1$

In the low-temperature phase $T<T_c$, the statistical properties of w_{max} and Y_2 have been studied in detail in [12]. In particular, the probability distribution $P_{T<T_c}(w_{max})$ coincides for $1/2<w_{max}\leqslant 1$ with the weight density $f(w)$ given in Eq. (14). Near the transition $\mu=T/T_c \to 1^-$, the singularity near w_{max} reads

$$P_{T<T_c}(w_{max}) = f_{T<T_c}(w_{max}) \underset{w_{max}\to 1}{\simeq} (1-\mu)(1-w_{max})^{\mu-1}. \tag{57}$$

In this section, we are interested in the behavior of the probability distribution $P_{T_c,N}(w_{max})$ near $w_{max} \to 1$ for finite samples at criticality,

$$P_{T_c,N}(w_{max}) = f_{T_c,N}(w_{max}) \underset{w_{max}\to 1}{\simeq} A_N(1-w_{max})^{\sigma}. \tag{58}$$

The same singularity governs the probability distribution of Y_2,

$$P_{T_c,N}(Y_2) \underset{Y_2\to 1}{\simeq} A_N(1-Y_2)^{\sigma}. \tag{59}$$

The amplitude A_N represents the global scaling of the rare samples which are still frozen, whereas the exponent σ describes the shape of the singularity. These rare events govern the disorder-averaged values $\overline{Y_k}$ at criticality [Eq. (13)], and for large k, the exponent σ governs the power-law dependence in k,

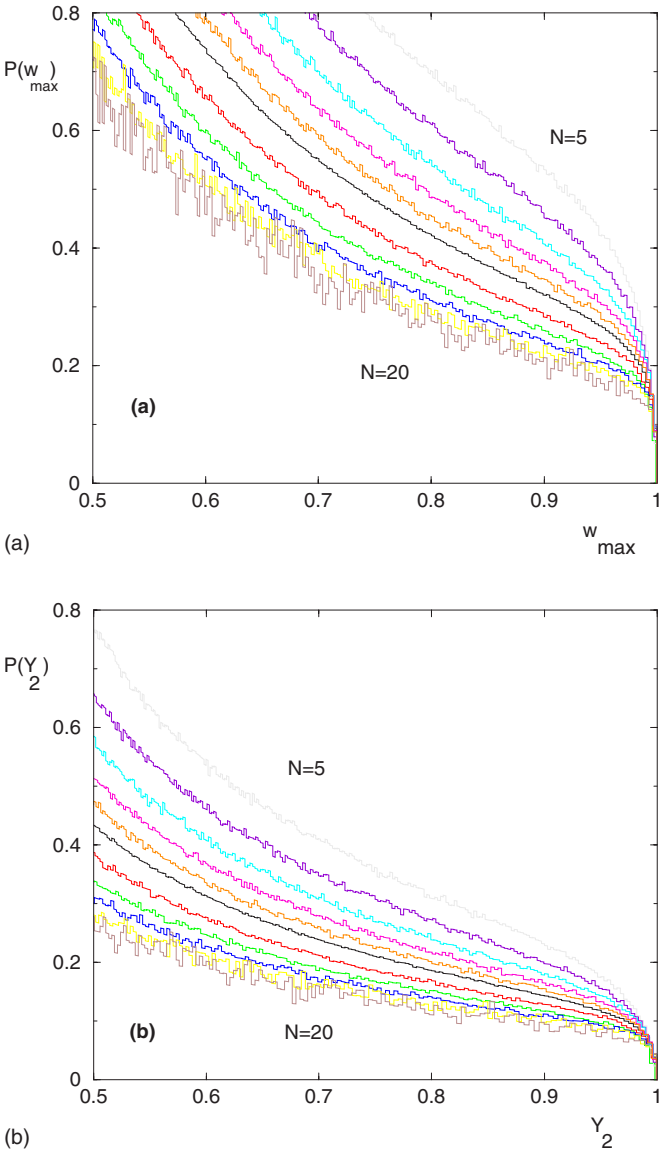

FIG. 8. (Color online) REM at criticality: Statistics of rare finite samples which are still frozen at T_c for sizes $N=5,6,7,8,9,10,12,14,16,18,20$. (a) Probability distribution of the maximal weight w_{max} in the region $1/2 \leqslant w_{max} \leqslant 1$. (b) Probability distribution of Y_2 in the region $1/2 \leqslant Y_2 \leqslant 1$.

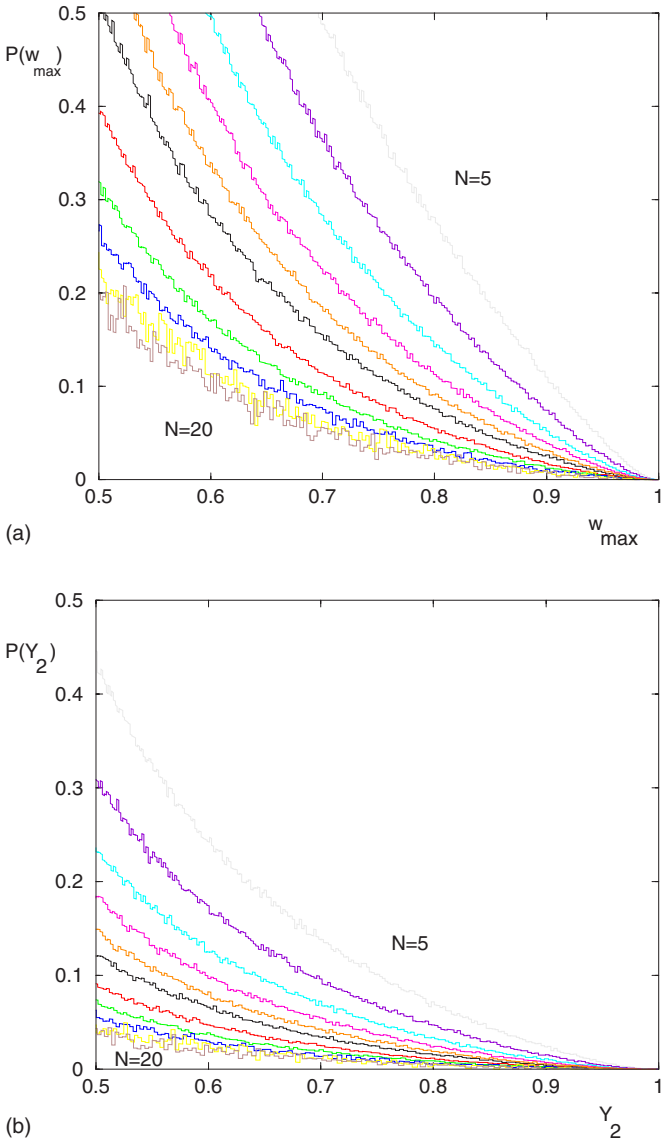

FIG. 9. (Color online) DPCT at criticality: Statistics of rare finite samples which are still frozen at T_c for sizes $N=5,6,7,8,9,10,12,14,16,18,20$. (a) Probability distribution of the maximal weight for sizes w_{max} in the region $1/2 \leqslant w_{max} \leqslant 1$; note the difference from the REM [Fig. 8(a) and 8(b)]. (b) Probability distribution of Y_2 in the region $1/2 \leqslant Y_2 \leqslant 1$; note the difference from the REM [Fig. 8(b)].

$$\overline{Y_k}(N) \underset{k\to\infty}{\propto} \frac{A_N}{k^{1+\sigma}}. \tag{60}$$

For the REM, where all finite-size scaling properties involve the factor $(T_c - T)N^{1/2}$, we expect

$$A_N^{REM} \underset{N\to\infty}{\propto} \frac{1}{N^{1/2}}, \tag{61}$$

$$\sigma_{REM} = 0. \tag{62}$$

This is in agreement via Eq. (60) with the leading behavior of the disorder-averaged values $\overline{Y_k}$ of Eq. (45). We show in Fig. 8 the behavior of the probability distributions of w_{max} and Y_2 near $w_{max} \to 1$ and $Y_2 \to 1$.

For the DPCT, the situation is more subtle. From the behavior in N of disorder-averaged values of Eq. (46), we conclude that the amplitude is governed by $\nu' = 1$,

$$A_N^{DPCT} \underset{N\to\infty}{\propto} \frac{1}{N}. \tag{63}$$

However, in contrast with the REM, the behavior of the probability distributions of w_{max} and Y_2 near $w_{max} \to 1$ and $Y_2 \to 1$ shown in Fig. 9 corresponds to a value $\sigma > 1$ for the singularity exponent. The measure of the k dependence of Eq. (60) indeed leads to a value of order

$$\sigma_{DPCT} \sim 1.5. \tag{64}$$

The fact that a finite σ appears at criticality for the DPCT, in contrast with the REM where $\sigma=0$ in continuity with the low-temperature phase, indicates that the tree structure plays a role at criticality, in contrast with the low-temperature phase, where the overlap distribution is concentrated on $q=0$ and 1 [Eq. (28)]. In the next section, we describe the finite-size properties of the overlap distribution at criticality.

VII. OVERLAP DISTRIBUTION AT CRITICALITY

In disorder-dominated phases, the order parameter is the "overlap" between two thermal configurations in the same disordered sample. In this section, we discuss in detail the overlap distribution for the DPCT, and compare with the REM case at the end.

For the DPCT, we consider the probability $P_N(t)$ that two walks of N steps have t common bonds in a fixed sample of a Cayley tree, where the possible values are $t=0,1,\ldots,N$. The normalization reads

$$\sum_{t=0}^{N} P_N(t) = 1. \tag{65}$$

The usual overlap distribution $\pi_N(q)$ concerning the fraction $q=t/N$ of common bonds reads

$$\pi_N(q) = NP_N(t = Nq) \tag{66}$$

with the normalization

$$\int_0^1 dq\ \pi_N(q) = 1. \tag{67}$$

A. Reminder of the overlap distribution for $T<T_c$ for the DPCT

As recalled in Eq. (28), the distribution of the overlap q between two walks on the same disordered tree is simply the sum of two δ peaks at $q=0$ and 1 in the whole low-temperature phase [7], and in particular the disorder average over the samples reads [Eq. (29)]

$$\bar{\pi}_{N=\infty}(q) = \frac{T}{T_c}\delta(q) + \left(1 - \frac{T}{T_c}\right)\delta(q-1). \tag{68}$$

The finite-size corrections have been studied in [16,17]: the probability $P_N(t)$ is finite at $t=0$ and N, whereas for $0 \ll t \ll N$, the disorder-averaged probability $P_N(t)$ obeys the scaling

$$\bar{P}_N(0<t<N) \underset{N\to\infty}{\propto} \frac{1}{N^{3/2}}\psi\left(\frac{t}{N}\right) \tag{69}$$

where the function $\psi(q)$ presents the singularities $q^{-3/2}$ and $(1-q)^{-3/2}$ near the two boundaries $q\to 0$ and $q\to 1$. For the finite-size overlap distribution, Eq. (69) translates into the finite-size correction

$$\bar{\pi}_N(0<q<1) \underset{N\to\infty}{\propto} \frac{1}{N^{1/2}}\psi(q) \tag{70}$$

to the asymptotic result of Eq. (68).

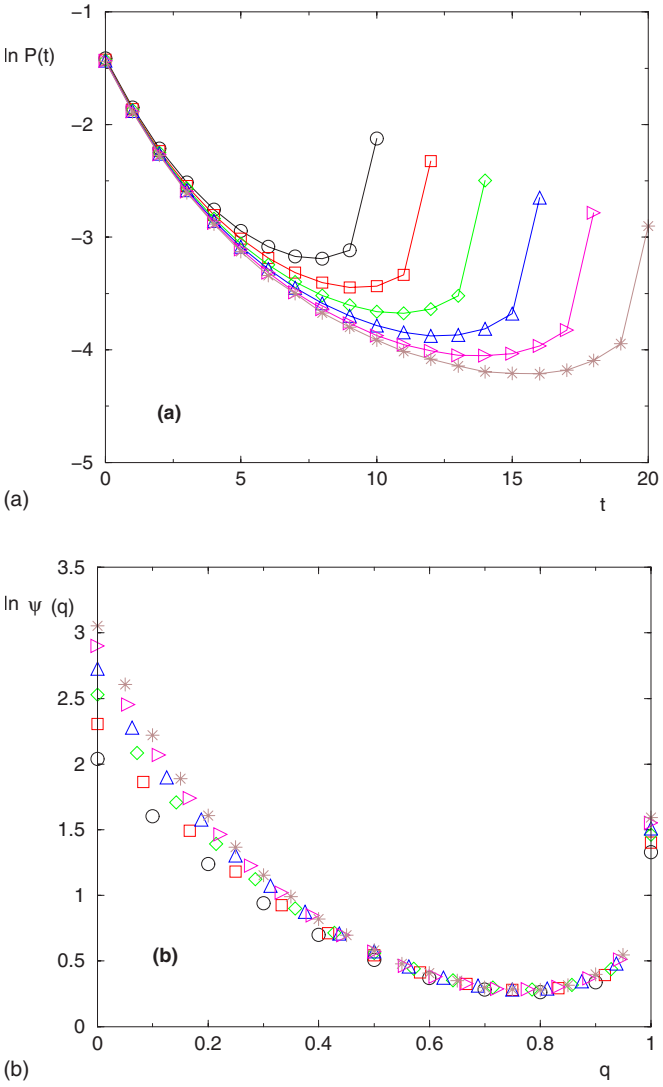

FIG. 10. (Color online) DPCT at criticality. (a) Logarithm of the disorder-averaged probability distribution $\bar{P}_N(t)$ of the number $t=0,1,\ldots,N$ of common bonds between two walks for sizes $N=10$ (○), 12 (□), 14 (◇), 16 (△), 18 (▷), 20 (∗). (b) Test of the scaling form of Eq. (73) for the disorder-averaged probability distribution $\bar{\pi}_N(q)$ of the overlap $0 \leqslant q=t/N \leqslant 1$: $\ln \psi(q) = \ln[N^{0.5}\bar{\pi}_N(q)]$ as a function of q.

B. Finite-size overlap distribution at T_c for the DPCT

In the limit $N\to\infty$, Eq. (68) becomes for $T=T_c$

$$\bar{\pi}_{T_c,N=\infty}(q) = \delta(q), \tag{71}$$

i.e., the whole normalization is concentrated on $q=0$. Here we are interested in the finite-size corrections to this result. We show in Figs. 10(a) and 10(b) the probability distributions $\bar{P}_{T_c,N}(t)$ and $\bar{\pi}_{T_c,N}(q)$ for various sizes. We now discuss the intermediate region $0<q<1$ and the two limit values $q=0$ and 1.

1. Region of intermediate overlap $0<q<1$

For $0<t<1$, we find numerically that the disorder-averaged probability $\bar{P}_N(t)$ obeys the scaling

$$\bar{P}_N(0 \ll t \ll N) \underset{N\to\infty}{\propto} \frac{1}{N^{1.5}} \psi\left(\frac{t}{N}\right) \tag{72}$$

or equivalently for the disorder-averaged overlap distribution $\bar{\pi}_N(q)$ of Eq. (66),

$$\bar{\pi}_N(0 < q < 1) \underset{N\to\infty}{\propto} \frac{1}{N^{0.5}} \psi(q) \tag{73}$$

as shown in Fig. 10(b).

2. Region of zero overlap $q=0$ at criticality

For finite t and $N\to\infty$, $\bar{P}_N(t)$ converge to finite values as shown in Fig. 10(a), in particular,

$$\bar{P}_N(t=0) \underset{N\to\infty}{\simeq} 0.23, \tag{74}$$

$$\bar{P}_N(t=1) \underset{N\to\infty}{\simeq} 0.15, \tag{75}$$

such that the normalization of these finite values corresponding to $q=0$ after rescaling, is 1 [Eq. (71)]. From the matching with the scaling regime of Eq. (72), one expects the following power-law decay for large t:

$$\bar{P}_{N=\infty}(t) \underset{t\to\infty}{\propto} \frac{1}{t^{1.5}}. \tag{76}$$

3. Probability of full overlap $q=1$ at criticality

By definition, the probability $P_N(N)$ of a full overlap $t=N$ coincides with the probability $Y_2=\Sigma w_i^2$ that the two walks end at the same point,

$$P_{T_c,N}(t=N) \equiv Y_2(N,T_c). \tag{77}$$

Using Eq. (43), the average over the samples yields

$$\bar{P}_{T_c,N}(N) \equiv \overline{Y_2}(N,T_c) \underset{N\to\infty}{\propto} \frac{1}{N}. \tag{78}$$

For the disorder-averaged overlap distribution of Eq. (66), we thus obtain that $\bar{\pi}_{T_c,N}(q=1)$ remains finite as $N\to\infty$:

$$\bar{\pi}_{T_c,N}(q=1) \underset{N\to\infty}{\simeq} \bar{\pi}_{N=\infty}(q=1) > 0. \tag{79}$$

In addition to the delta function $\delta(q)$ which bears the whole normalization [Eq. (71)], the asymptotic probability distribution $\bar{\pi}_{N=\infty}(q)$ of the overlap q thus contains an isolated point at $q=1$ where $\bar{\pi}_{N=\infty}(q=1)>0$. This finite value at $q=1$ is due to rare events, since the typical value at $q=1$ is of order [Eq. (51)]

$$\pi^{typ}_{T_c,N}(q=1) = NY_2^{typ}(N,T_c) \underset{N\to\infty}{\propto} \frac{1}{N}. \tag{80}$$

We show in Fig. 11(a) the probability $P_{T_c,N}(\pi(q=1))$ over the samples of the probability density $\pi_N(q=1)$ of full overlap between two configurations. From the probability of rare events with $Y_2\to 1$ of Eq. (59), one obtains via the change of variables $\pi_N(q=1)=NY_2$ the following singularity near the maximal value $\pi(q=1)\to N$:

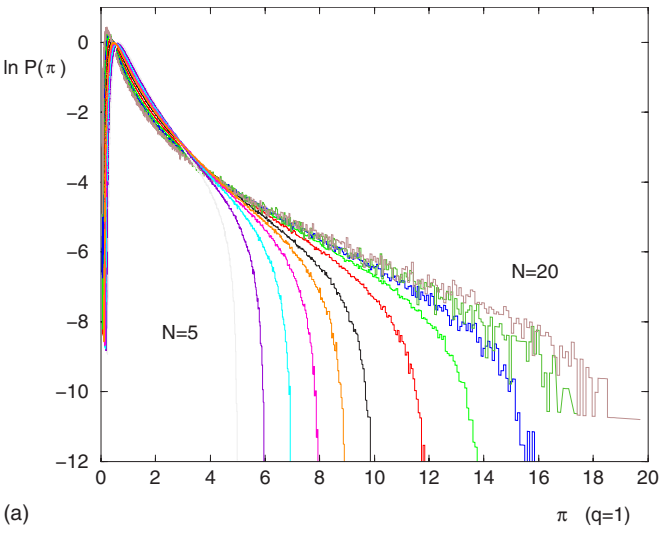

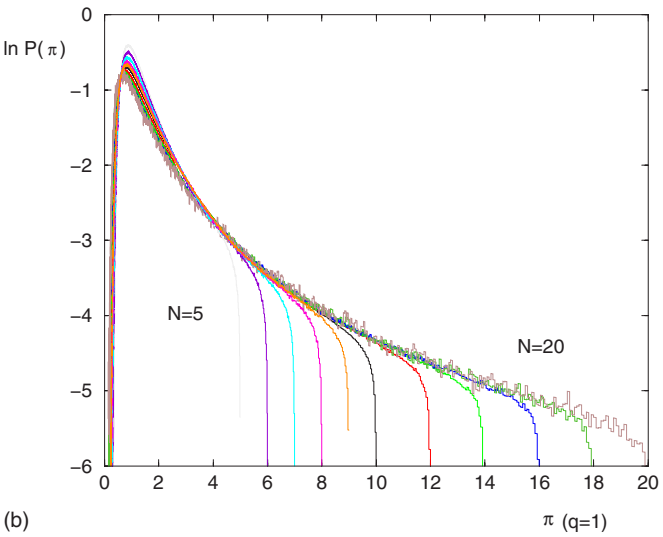

FIG. 11. (Color online) Statistics over the samples of the probability density $\pi(q=1)$ of full overlap between two configurations at criticality, for sizes $N=5,6,7,8,9,10,12,14,16,18,20$. (a) Logarithm of the probability distribution $P(\pi(q=1))$ for the DPCT. (b) Logarithm of the probability distribution $P(\pi(q=1))$ for the REM.

$$P_{T_c,N}(\pi(q=1)) \underset{\pi(q=1)\to N}{\simeq} \frac{A_N}{N^{1+\sigma}}[N-\pi(q=1)]^{\sigma} \tag{81}$$

where $A_N^{(DPCT)} \propto 1/N$ and $\sigma_{DPCT} \sim 1.5$.

C. Overlap distribution at criticality in the REM

In the REM with N spins, the spin overlap

$$t = \sum_{i=1}^{N} S_i^{(1)} S_i^{(2)} \tag{82}$$

can be defined from its relation with the p-spin-glass model [13,14] in the limit $p\to\infty$. It is $t=N$ if the two configurations

are identical, $\mathcal{C}^{(1)}=\mathcal{C}^{(2)}$, and $t<N$ if the two configurations are different, $\mathcal{C}^{(1)}\neq\mathcal{C}^{(2)}$.

As in Eq. (78), the probability $P_N(N)$ of a full overlap $t=N$ coincides with the probability $Y_2=\Sigma w_i^2$ that the two configurations are the same. Using Eq. (42), the average over the samples yields

$$\bar{P}^{REM}_{T_c,N}(N)\equiv\overline{Y_2}(N,T_c)\underset{N\to\infty}{\propto}\frac{1}{N^{1/2}}. \tag{83}$$

For the overlap distribution of Eq. (66), we thus obtain that $\bar{\pi}_{T_c,N}(q=1)$ diverges as $N\to\infty$,

$$\bar{\pi}^{REM}_{T_c,N}(q=1)\underset{N\to\infty}{\simeq}N^{1/2}. \tag{84}$$

In addition to the delta function $\delta(q)$ which bears the whole normalization [Eq. (71)], the asymptotic probability distribution $\bar{\pi}_{N=\infty}(q)$ of the overlap q thus contains an isolated point at infinity as a memory of the delta peak $(1-T/T_c)\delta(q-1)$ of the low-temperature phase $T<T_c$. Again this divergence at $q=1$ is due to rare events. However here, in contrast with the directed polymer [Eq. (80)], the typical value at $q=1$ remains finite [Eq. (50)],

$$\pi^{typ}_{T_c,N}(q=1)=NY_2^{typ}(N,T_c)\simeq\text{const}. \tag{85}$$

We show in Fig. 11(b) the probability $P_{T_c,N}(\pi(q=1))$ over the samples of the probability density $\pi_N(q=1)$ of full overlap between two configurations. The singularity near the maximal value is given by Eq. (81) where $A_N^{(REM)}\propto 1/N^{1/2}$ and $\sigma_{REM}=0$.

VIII. CONCLUSION

In this paper, we have studied the weight statistics at criticality for the random energy model and for the directed polymer on a Cayley tree with random bond energies. These two mean-field disordered models present freezing transitions with similar thermodynamic properties. In particular, between the high-temperature phase of extensive entropy and the low-temperature phase of finite entropy, the entropy at criticality scales as $\bar{S}_N(T_c)\sim N^{1/2}$ in both models. However, the statistical properties of the weights, which coincide in the low-temperature phase, become different at the critical point. In the REM, all critical properties are governed by the finite-size exponent $\nu=2$: the typical values $e^{\overline{\ln Y_k}}$ decay as $N^{-k/2}$, and the disorder-averaged values $\overline{Y_k}$ are governed by rare events and decay as $N^{-1/2}$ for any $k>1$. In the DPCT, we find that the weight statistics is not governed by the exponent $\nu=2$ of the thermodynamics, but by another exponent $\nu'=1$ that had been previously mentioned in [8] in connection with finite-size corrections to the free energy below and at T_c. In particular, the typical values $e^{\overline{\ln Y_k}}$ decay as N^{-k}, and the disorder-averaged values $\overline{Y_k}$ decay as N^{-1} for any $k>1$. We have also presented numerical histograms at criticality for the entropy, the maximal weight w_{max} and Y_2. We have emphasized the role of the rare samples that are still frozen at T_c (i.e., the rare samples having $S\sim 0$, $w_{max}\sim 1$, $Y_2\sim 1$) since it is the amplitude of these rare events that governs the disorder-averaged values $\overline{Y_k}$ as well as the overlap probability density $\bar{\pi}_{T_c,N}(q=1)$ of full overlap $q=1$. In particular, we have obtained the result that, in addition to the delta function $\delta(q)$ which bears the whole normalization, the disorder-averaged asymptotic probability distribution $\bar{\pi}_{T_c,N=\infty}(q)$ contains an isolated point at $q=1$ as a memory of the delta peak $(1-T/T_c)\delta(q-1)$ of the low-temperature phase $T<T_c$. The associated value $\bar{\pi}_{N=\infty}(q=1)$ is finite for the DPCT, and diverges as $\bar{\pi}_{N=\infty}(q=1)\sim N^{1/2}$ for the REM.

Concerning the weight statistics at criticality for the directed polymer, let us finish by some comparison between the mean-field version on the Cayley tree considered here and the finite-dimensional version that we have studied recently in [4]. We should first recall that, in finite dimension d, the weights of the $O(N^d)$ possible spatial positions of the polymer end point do not coincide with the configuration weights, in contrast with the Cayley tree, where the end points are in one-to-one correspondence with the 2^N configurations. In finite dimension, the probability distributions of the maximal weight w_{max} and of Y_2 reach the values $w_{max}=1$ and $Y_2=1$ only for $T\leqslant T_{gap}$, where $T_{gap}<T_c$ [18], whereas on the Cayley tree these two temperatures coincide, $T_{gap}=T_c$. This is why, on the Cayley tree, the disorder-averaged values $\overline{Y_k}$ for $k>1$ all decay with a k-independent exponent $\overline{Y_k}\propto 1/N$ representing the amplitude of rare events where $w_{max}\sim 1$, whereas in finite dimension, the disorder-averaged values $\overline{Y_k}$ decay as $\overline{Y_k}\propto 1/N^{(k-1)\tilde{D}(k)}$, where the exponents $\tilde{D}(k)$ have a finite limit $\tilde{D}(+\infty)>0$. Also, in finite dimension, the comparison with the exponents $D(k)$ governing the decay of typical values $Y_k^{typ}=e^{\overline{\ln Y_k}}\propto 1/N^{(k-1)D(k)}$ shows that the threshold k_c between the region $k\leqslant k_c$, where they coincide, $D(k)=\tilde{D}(k)$, and the region $k>k_c$, where they differ, $D(k)>\tilde{D}(k)$, is of order $k_c\sim 2$ [4], whereas on the Cayley tree the exponents for averaged and typical values are always different as soon as $k>1$. So the role of rare events is stronger on the Cayley tree.

APPENDIX A: LÉVY SUMS FOR $\mu<1$

In this appendix, we recall some properties of Lévy sums with $\mu<1$, since their weight statistics is the same as in the random energy model in the low-temperature phase with $\mu(T)=T/T_c$.

1. Weight statistics in Lévy sums

The sum

$$\Sigma_M=\sum_{i=1}^{M}x_i \tag{A1}$$

of M positive independent variables $(x_1,\ldots,x_M)$ distributed with a probability distribution that decays algebraically

$$\rho(x)\underset{x\to+\infty}{\simeq}\frac{A}{x^{1+\mu}} \tag{A2}$$

has a very special property when $0<\mu<1$ since the first moment diverges, $\langle x\rangle=+\infty$ [13,19]: the sum Σ_M grows as

$M^{1/\mu}$, and the rescaled variable is distributed with a stable Lévy distribution. Another important property is that the maximal variable $x_{max}(M)$ among the M variables $(x_1, \ldots, x_M)$ is also of order $M^{1/\mu}$, i.e., the sum Σ_M is actually dominated by the few biggest terms. To quantify this effect, it is convenient to introduce the weights

$$w_i = \frac{x_i}{\Sigma_M} \tag{A3}$$

and their moments

$$Y_k = \sum_{i=1}^{M} w_i^k. \tag{A4}$$

The link with the weight statistics in the random energy model can be understood as follows. The lowest energy in the REM is distributed exponentially,

$$P_{extremal}(E) \underset{E \to -\infty}{\simeq} e^{\gamma E}. \tag{A5}$$

This exponential form, which corresponds to the tail of the Gumbel distribution for extreme-value statistics [20,21], immediately yields that the Boltzmann weight $x=e^{-\beta E}$ has a distribution that decays algebraically [Eq. (A2)] with exponent

$$\mu = T\gamma. \tag{A6}$$

In the REM, the coefficient γ in the exponential [Eq. (A5)] is $\gamma = 1/T_c$.

Let us also mention that in the mean-field Sherrington-Kirkpatrick (SK) model of spin glasses, exactly the same expressions for Y_k [Eq. (A8)] also appear [2,22], but with a different interpretation: the weights are those of the pure states. As a consequence, the parameter $\mu(T)$, which is a complicated function of the temperature, vanishes at the transition $\mu(T_c)=0$ (only one pure state in the high-temperature state) and grows as T is lowered toward $\mu(T=0)$ of order 0.5 [23]. This is in contrast with the REM model where $\mu(T) = T/T_c$ grows with the temperature from $\mu(T=0)=0$ (only one ground state) to $\mu(T_c)=1$ at the transition, where the number of important microscopic states is no longer finite. Nevertheless, the expression [Eq. (A8)] for the weights of pure states means that the free energy f of pure states in the SK model is distributed exponentially,

$$P(f) \underset{f \to -\infty}{\simeq} e^{\gamma(T) f}, \tag{A7}$$

with a parameter $\gamma(T) = \mu(T)/T$.

2. Disorder-averaged moments $\overline{Y_k}^{Lévy}$

The averaged values in the limit $M \to \infty$ are finite for $0 < \mu < 1$ and read [13]

$$\overline{Y_k}^{Lévy} = \frac{\Gamma(k-\mu)}{\Gamma(k)\Gamma(1-\mu)}. \tag{A8}$$

Let us recall how one derives this result [13], since it will be useful for the critical case $\mu_c = 1$ considered in Appendix B. It is convenient to exponentiate the denominator according to [13]

$$Y_k = \frac{1}{\Gamma(k)} \int_0^{+\infty} dt\, t^{k-1} \exp\left(-t \sum_i x_i^k\right) \sum_j x_j^k \tag{A9}$$

in order to perform the average

$$\overline{Y_k}^{Lévy} = \frac{M}{\Gamma(k)} \int_0^{+\infty} dt\, t^{k-1}\, \overline{x^k e^{-tx}}\, (\overline{e^{-tx}})^{M-1}. \tag{A10}$$

For large M, the integral will be dominated by the region where t is small, and one may approximate [13]

$$\overline{x^k e^{-tx}} = \int dx\, \rho(x) x^k e^{-tx} \sim A t^{\mu-k} \Gamma(k-\mu) \tag{A11}$$

and

$$\overline{e^{-tx}} = \int dx\, \rho(x) e^{-tx} \sim e^{-t^\mu A[-\Gamma(-\mu)]}, \tag{A12}$$

yielding

$$\overline{Y_k}^{Lévy} = \frac{MA\Gamma(k-\mu)}{\Gamma(k)} \int_0^{+\infty} dt\, t^{\mu-1} e^{-Mt^\mu A[-\Gamma(-\mu)]}, \tag{A13}$$

leading to Eq. (A8) in the limit $M \to \infty$. More generally, correlation functions between Y_k can also be computed [13], in particular,

$$\overline{Y_k^2}^{Lévy} = \frac{1}{\Gamma(2k)} \left(\frac{\Gamma(2k-\mu)}{\Gamma(1-\mu)} + \mu \frac{\Gamma^2(k-\mu)}{\Gamma^2(1-\mu)} \right). \tag{A14}$$

3. Typical values $Y_k^{Lévy}(\mathrm{typ}) = e^{\overline{\ln Y_k}}$

To compute the disorder average of the logarithm of Y_k, we first rewrite

$$\ln Y_k = \ln\left(\sum_{i=1}^{M} x_i^k\right) - k \ln\left(\sum_{i=1}^{M} x_i\right) \tag{A15}$$

and use the identity

$$\ln Z = \int_0^{+\infty} \frac{dt}{t} (e^{-t} - e^{-tZ}) = \lim_{\epsilon \to 0} \left(\int_0^{+\infty} dt\, t^{\epsilon-1} e^{-t} - \int_0^{+\infty} dt\, t^{\epsilon-1} e^{-tZ} \right). \tag{A16}$$

Using Eq. (A12), we obtain

$$\overline{\ln\left(\sum_{i=1}^{M} x_i\right)} = \int_0^{+\infty} \frac{dt}{t} [e^{-t} - (\overline{e^{-tx}})^M] \sim \left(1 - \frac{1}{\mu}\right) \Gamma'(1) + \frac{1}{\mu} \ln\{MA[-\Gamma(-\mu)]\}, \tag{A17}$$

and similarly

$$\overline{\ln\left(\sum_{i=1}^{M} x_i^k\right)} = \int_0^{+\infty} \frac{dt}{t}[e^{-t} - (\overline{e^{-tx^k}})^M] \sim \left(1 - \frac{k}{\mu}\right)\Gamma'(1) + \frac{k}{\mu}\ln\left\{M\frac{A}{k}\left[-\Gamma\left(-\frac{\mu}{k}\right)\right]\right\}, \quad \text{(A18)}$$

so that finally in the limit $M \to \infty$ [Eq. (A15)]

$$\overline{\ln Y_k} = (1-k)\Gamma'(1) + \frac{k}{\mu}\ln\left(\frac{\Gamma(1-\mu/k)}{\Gamma(1-\mu)}\right). \quad \text{(A19)}$$

4. Critical behaviors near the transition point $\mu \to \mu_c = 1$

As $\mu \to 1$, Eq. (A19) gives the following leading term:

$$\overline{\ln Y_k} \sim k \ln(1-\mu), \quad \text{(A20)}$$

i.e., the typical values vanish as

$$Y_k^{Lévy}(\text{typ}) = e^{\overline{\ln Y_k}} \sim (1-\mu)^k, \quad \text{(A21)}$$

whereas the averaged moments of Eq. (A8) vanish linearly as

$$\overline{Y_k}^{Lévy} = \frac{(1-\mu)}{k-1} + O((1-\mu)^2), \quad \text{(A22)}$$

as well as higher moments, for instance, Eq. (14),

$$\overline{Y_k^2}^{Lévy} \sim \frac{(1-\mu)}{2k-1} + O((1-\mu)^2). \quad \text{(A23)}$$

This shows that disorder-averaged values are governed by the rare events where the maximal weight w_{max} is near 1: the density $f(w)$ of Eq. (14) becomes for $\mu \to 1$

$$f_{Lévy}(w) \underset{\mu \to 1}{\simeq} (1-\mu) w^{-1-\mu}(1-w)^{\mu-1}. \quad \text{(A24)}$$

APPENDIX B: WEIGHT STATISTICS FOR LÉVY SUMS AT CRITICALITY $\mu_c = 1$

In this appendix, we describe some results on the weight statistics for Lévy sums at criticality $\mu_c = 1$ to compare with the results given in the text for the random energy model and for the directed polymer on a Cayley tree. For $\mu_c = 1$, the sum Σ_M of Eq. (A1) scales as $M \ln M$, whereas the maximal value x_{max} among the M variables scales as M [19]: the decay of the Y_k is thus expected to depend on the variable $(\ln M)$.

1. Decay of disorder-averaged values $\overline{Y_k}(M)$

We start from Eq. (A10),

$$\overline{Y_k} = \frac{M}{\Gamma(k)} \int_0^{+\infty} dt\, t^{k-1} \overline{x^k e^{-tx}} (\overline{e^{-tx}})^{M-1}. \quad \text{(B1)}$$

For large M, the integral will be dominated by the region where t is small, and one may approximate

$$\overline{x^k e^{-tx}} = \int dx\, \rho(x) x^k e^{-tx} \sim A t^{1-k}\Gamma(k-1) \quad \text{(B2)}$$

and

$$\overline{e^{-tx}} = \int dx\, \rho(x) e^{-tx} \sim e^{-At\ln(1/t)}, \quad \text{(B3)}$$

yielding

$$\overline{Y_k} = \frac{MA}{k-1}\int_0^{+\infty} dt\, e^{-MAt\ln(1/t)} \sim \frac{1}{(k-1)\ln M}. \quad \text{(B4)}$$

2. Disorder-averaged entropy

From Eq. (B1), the disorder-averaged entropy [Eq. (17)] reads

$$\overline{S(M)} = -\partial_k Y_k|_{k=1} = M\int_0^{+\infty} dt(\overline{e^{-tx}})^{M-1} \int dx\, \rho(x)\{[\Gamma'(1) - \ln t - \ln x]xe^{-tx}\}. \quad \text{(B5)}$$

Using Eq. (B3), one obtains at leading order

$$\overline{S(M)} \propto \ln(MA\ln M). \quad \text{(B6)}$$

3. Decay of typical values $Y_k^{typ}(M) = e^{\overline{\ln Y_k}}$

To compute the disorder average of the logarithm of Y_k, we start from Eqs. (A15) and (A16). Using Eq. (B3), we obtain

$$\overline{\ln\left(\sum_{i=1}^{M} x_i\right)} = \int_0^{+\infty} \frac{dt}{t}[e^{-t} - (\overline{e^{-tx}})^M] \sim \int_0^{+\infty} \frac{dt}{t}(e^{-t} - e^{-MAt\ln(1/t)}) \sim \ln(MA\ln M), \quad \text{(B7)}$$

and as in Eq. (A18) with $\mu = 1$

$$\overline{\ln\left(\sum_{i=1}^{M} x_i^k\right)} = \int_0^{+\infty} \frac{dt}{t}[e^{-t} - (\overline{e^{-tx^k}})^M] \sim (1-k)\Gamma'(1) + k\ln\left\{M\frac{A}{k}\left[-\Gamma\left(-\frac{1}{k}\right)\right]\right\}, \quad \text{(B8)}$$

so that finally the leading term is [Eq. (A15)]

$$\overline{\ln Y_k} = \overline{\ln\left(\sum_{i=1}^{M} x_i^k\right)} - k\,\overline{\ln\left(\sum_{i=1}^{M} x_i\right)} \sim -k\ln(\ln M), \quad \text{(B9)}$$

i.e.,

$$Y_k^{\text{typ}}(M) = e^{\overline{\ln Y_k}} \sim \frac{1}{(\ln M)^k}. \quad \text{(B10)}$$

4. Finite-size scaling in the critical region

The comparison of the results for the entropy, for the disorder-averaged values, and for the typical values of the Y_k between the phase $\mu < 1$ and the critical point $\mu_c = 1$ shows that the appropriate scaling variable is $(1-\mu)\ln M$, corresponding to a finite-size exponent

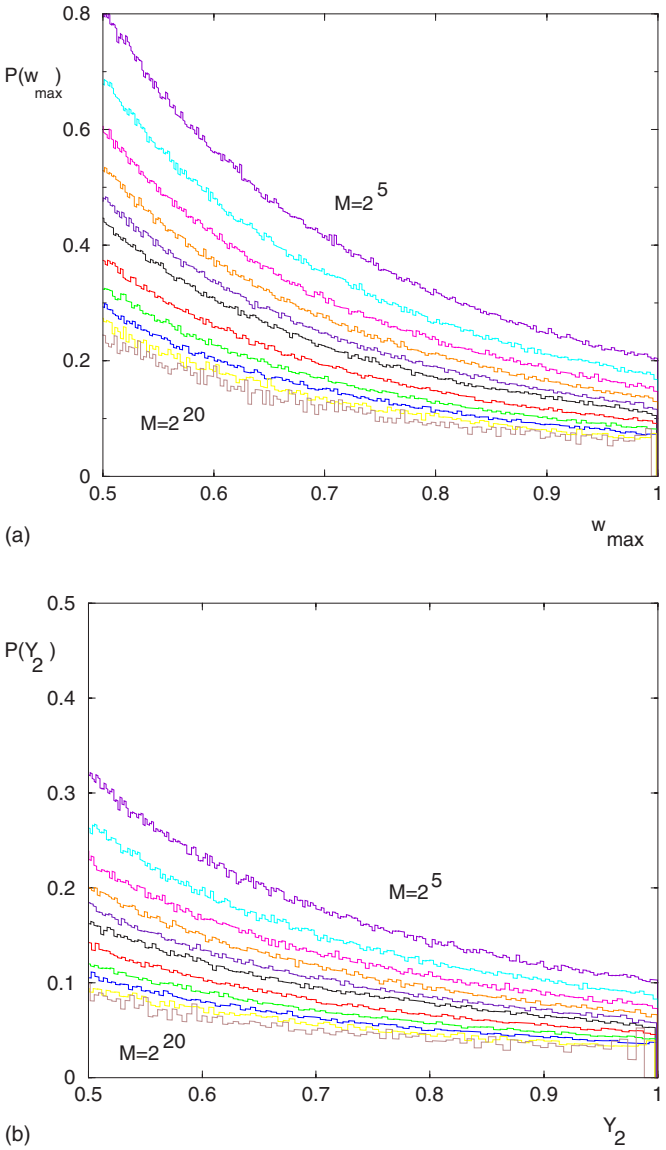

FIG. 12. (Color online) Weight statistics in Lévy sums of M terms (with $2^5 \leqslant M \leqslant 2^{20}$) for the critical value $\mu_c = 1$. (a) Probability distribution of the maximal weight w_{max} in the region $1/2 \leqslant w_{max} \leqslant 1$. (b) Probability distribution of Y_2 in the region $1/2 \leqslant Y_2 \leqslant 1$.

$$\nu_{Lévy} = 1. \tag{B11}$$

This is in contrast with the random energy model, where the number of configurations is $M = 2^N$, and the appropriate finite-size scaling behavior [Eq. (30)] is $(T_c - T)N^{1/2} = (1 - \mu)(\ln M)^{1/2}$ with $\nu_{REM} = 2$.

5. Probability distributions of w_{max} and of Y_2

We show in Fig. 12 the finite-size probability distributions of the maximal weight w_{max} and Y_2 at the critical value $\mu_c = 1$, to compare with the corresponding figures given in the text for the REM (Fig. 8) and for the DPCT (Fig. 9) with the correspondence $M = 2^N$. As in Eq. (58), the behavior of the probability distribution $P_{\mu_c,M}(w_{max})$ near $w_{max} \to 1$ for finite sums of M terms at the critical value $\mu_c = 1$ is of the form

$$P_{\mu_c,M}(w_{max}) \underset{w_{max} \to 1}{\simeq} A_M (1 - w_{max})^{\sigma}. \tag{B12}$$

The amplitude A_M of these rare events is the amplitude that governs the disorder-averaged values $\overline{Y_k}$ of Eq. (B4),

$$A_M \underset{M \to \infty}{\propto} \frac{1}{\ln M}. \tag{B13}$$

The singularity exponent σ is simply

$$\sigma_{Lévy} = 0 \tag{B14}$$

in continuity with the rare events in the region $\mu < 1$. This value is the same as in the REM [Eq. (62)] but different from the value measured in the DPCT [Eq. (64)].

6. Conclusion: Comparison with the REM and the DPCT

In this appendix, we have described the weight statistics in Lévy sums for the critical value $\mu_c = 1$, to compare with the REM and the DPCT cases studied in the text. Although the three models have the same properties in the low-temperature phase with $\mu = T/T_c < 1$, we find here that the three models have different critical finite-size properties. The REM and the Lévy sums involve a single finite-size exponent,

$$\nu_{REM} = 2, \tag{B15}$$

$$\nu_{Lévy} = 1, \tag{B16}$$

and both have a singularity exponent

$$\sigma_{REM} = 0 = \sigma_{Lévy}, \tag{B17}$$

in continuity with its low-temperature value $\sigma = \mu - 1 \to 0$. On the contrary, the DPCT involves two exponents

$$\nu_{DPCT} = 2, \tag{B18}$$

$$\nu'_{DPCT} = 1. \tag{B19}$$

The exponent $\nu = 2$ governs the thermodynamics, in particular the entropy and the specific heat, whereas $\nu' = 1$ governs the Y_k statistics. Moreover, the singularity exponent at criticality,

$$\sigma_{DPCT} \simeq 1.5, \tag{B20}$$

is very different from the limit of its low-temperature value $\sigma = T/T_c - 1 \to 0$.

[1] K. Binder and A. P. Young, Rev. Mod. Phys. **58**, 801 (1986).
[2] M. Mézard, G. Parisi, and M. A. Virasoro, *Spin Glass Theory and Beyond* (World Scientific, Singapore, 1987).
[3] T. Halpin-Healy and Y.-C. Zhang, Phys. Rep. **254**, 215 (1995).
[4] C. Monthus and T. Garel, arXiv:cond-mat/0701699, Phys. Rev. E (to be published).
[5] F. Wegner, Z. Phys. B **36**, 209 (1980); C. Castellani and L. Peliti, J. Phys. A **19**, L429 (1986); M. Janssen, Int. J. Mod. Phys. B **8**, 943 (1994); M. Janssen, Phys. Rep. **295**, 1 (1998); B. Huckestein, Rev. Mod. Phys. **67**, 357 (1995).
[6] F. Evers and A. D. Mirlin, Phys. Rev. Lett. **84**, 3690 (2000); A. D. Mirlin and F. Evers, Phys. Rev. B **62**, 7920 (2000); F. Evers, A. Mildenberger, and A. D. Mirlin, *ibid.* **64**, 241303 (2001); A. Mildenberger, F. Evers, and A. D. Mirlin, *ibid.* **66**, 033109 (2002); A. D. Mirlin, Y. V. Fyodorov, A. Mildenberger, and F. Evers, Phys. Rev. Lett. **97**, 046803 (2006).
[7] B. Derrida and H. Spohn, J. Stat. Phys. **51**, 817 (1988).
[8] J. Cook and B. Derrida, J. Stat. Phys. **63**, 505 (1991).
[9] S. N. Majumdar and P. L. Krapivsky, Phys. Rev. E **62**, 7735 (2000); **65**, 036127 (2002); D. S. Dean and S. N. Majumdar, *ibid.* **64**, 046121 (2001).
[10] B. Derrida, Phys. Rev. B **24**, 2613 (1981).
[11] B. Derrida and G. Toulouse, J. Phys. (France) Lett. **46**, L223 (1985).
[12] B. Derrida and H. Flyvbjerg, J. Phys. A **20**, 5273 (1987).
[13] B. Derrida, in *On Three Levels*, edited by M. Fannes *et al.* (Plenum Press, New York, 1994).
[14] D. J. Gross and M. Mézard, Nucl. Phys. B **240**, 431 (1984).
[15] A. Bovier, I. Kurkova, and M. Löwe, Ann. Probab. **30**, 605 (2002).
[16] D. S. Fisher and D. A. Huse, Phys. Rev. B **B43**, 10728 (1991).
[17] L. H. Tang, J. Stat. Phys. **77**, 581 (1994).
[18] C. Monthus and T. Garel, J. Stat. Mech.: Theory Exp. (2007) P03011.
[19] J. P. Bouchaud and A. Georges, Phys. Rep. **195**, 127 (1990).
[20] E. J. Gumbel, *Statistics of Extreme* (Columbia University Press, New York, 1958); J. Galambos, *The Asymptotic Theory of Extreme Order Statistics* (Krieger, Malabar, FL, 1987).
[21] J. P. Bouchaud and M. Mzard, J. Phys. A **30**, 7997 (1997).
[22] M. Mézard, G. Parisi, and M. A. Virasoro, J. Phys. (France) Lett. **46**, L217 (1985).
[23] J. Vannimenus, G. Toulouse, and G. Parisi, J. Phys. (France) **42**, 565 (1981); A. Crisanti, T. Rizzo, T. Temesvari, Eur. Phys. J. B **33**, 203 (2003).